JOURNAL OF SPACECRAFT AND ROCKETS
Vol. 33, No. 6, November–December 1996

Weight Optimization for Honeycomb Radiators with Embedded Heat Pipes

David G. T. Curran* and Tung T. Lam†
The Aerospace Corporation, El Segundo, California 90245-4691

A mathematical model for a single-stage space radiator with embedded heat pipes has been developed, and graphical solutions are presented for tradeoff studies. The model allows selection of the optimum radiator sizing for spacecraft payload heat rejection. It calculates the minimum weight configuration for specified radiator parameters involving temperature, heat pipe, and honeycomb panel characteristics such as heat pipe spacing and facesheet thickness, as well as radiative surface properties and panel thermal conductivities. The data in terms of graphical form are applicable to practical engineering design applications.

Nomenclature

A_R = radiator area, m^2
C_0 = $\varepsilon\sigma T_R^3/k_F t_F$, m^{-2}
C_1 = heat pipe-adhesive weight per unit length, $W_{HP} + 4L_P(\rho t)_{HPADH}$, kg/m
C_2 = facesheet, coating-adhesive, and shielding weight per unit length, $2(\rho t)_{FSH} + (\rho t)_{OSR} + (\rho t)_{OSRADH} + (\rho t)_{AR}$, kg/m
C_3 = honeycomb-adhesive weight per unit length, $2(\rho t)_{HC} + 4f(\rho t)_{HCADH}$, kg/m
E = planetary emission
F = view factor
f = adhesive filling factor at honeycomb interface
k = thermal conductivity, W/m-°C
L = length, m
L_F = fin section length, m
L_P = heat pipe section length, m
L_R = radiator length, m
ℓ = heat pipe spacing, $2(L_P + L_F)$, m
N = integer number of heat pipes, $\leq L_R/\ell$
q = heat rejection, kW
S = solar constant, W/m^2
T = temperature, °C
T_R = heat pipe temperature in contact with facesheet (fin root temperature), °C
T_s = equivalent sink temperature, °C
t = thickness, m
W = weight, kg
W_{HP} = heat pipe weight per length, kg/m
α_s = solar absorptance
ε = emittance
η = fin effectiveness
θ = T_s/T_R
θ_s = solar incidence angle, deg
λ = $C_0 L_F^2$
ρ = material density, kg/m^3
ρ = reflectance
σ = Stefan–Boltzmann constant, 5.673E-11 kW/m^2-K^4

Subscripts

A = albedo
ADH = adhesive bond between components
AR = armor (shielding)
F = fin
FSH = facesheet
HC = honeycomb
HP = heat pipe
IR = infrared
i = satellite appendages
OSR = optical solar reflector
R = radiator
s = sink
W = width

Presented as Paper 95-2136 at the AIAA 30th Thermophysics Conference, San Diego, CA, June 19–22, 1995; received Feb. 28, 1996; revision received June 18, 1996; accepted for publication June 21, 1996.

*Senior Member, Technical Staff, Cryogenics Section, Vehicle Systems Division.
†Manager, Satellite Heat Transfer Section, Vehicle Systems Division. Associate Fellow AIAA.

Introduction

THIS is a challenging time for the space industry in the commercial sector in general and the defense establishment in particular. As the defense budget continues to drop in the foreseeable future, the fierce competition among the aerospace manufacturers and the pressures to build lighter, cheaper, and better spacecraft are enormous. There is a direct link between the weight of the spacecraft and the cost of the launch vehicle. Hence, cost reduction of a satellite program is achievable through weight reduction. It is, therefore, advantageous to reduce future satellite weight to a medium launch vehicle capability such as an Atlas IIAS class launch vehicle or smaller. The future trend in satellite design is to develop smaller satellites with a common or standard bus. As a result, the system cost will be reduced through use of a common/modular spacecraft bus. Advanced spacecraft technologies will tend to be applicable to all of the satellites, independent of the payload. Additionally, the miniaturization program also demands increased capabilities of the space system. Some of the key issues space system designers will have to face include improving system efficiency while maintaining high reliability to avoid mission failures.

The challenge for thermal engineers is to reduce both the weight of the thermal control system and required heater power while maintaining temperature control of critical equipment for enhanced performance and increased reliability. Current spacecraft thermal design uses localized thermal control techniques, such as multilayer insulation blankets, heat sinks/doublers, surface coatings, heat pipes, louvers, heaters, and radiators. Proper thermal control has to be applied to individual payload and electronics design based on detailed analyses. The future common/modular spacecraft bus design and improved radiator heat rejection through materials improvements and contamination control will accommodate a wide range of component locations and power levels with an adaptive thermal control subsystem.

In the past two decades thermal control hardware has been improved, although slowly, to accommodate trends in the industry for high powered spacecraft.[1] One of the technologies developed includes the use of a honeycomb radiator panel with embedded heat

pipe for spacecraft thermal control.[2,3] The aim is to develop a radiator optimization program that can be used for thermal technology tradeoff studies. The parameters studied included the effects of minimizing solar loads through modifying solar absorptance and emittance of radiator coatings, weight impact of thermal margins, and weight effects of radiator facesheet materials such as composites vs the standard aluminum facesheet. The minimum weight and the corresponding radiator area are determined on a per unit heat rejection basis (kilograms per kilowatt and square meters per kilowatt) from these parameter variations.

Problem Formulation

Figure 1 depicts a single-stage space radiator with embedded heat pipes. Because of the symmetry of the physical configuration, the present study is focused on a section of the radiator. The total weight of the radiator under consideration consists of the weights of the heat pipe per unit length, facesheets, adhesive bond between heat pipe and facesheets, optical solar reflector (OSR) and bonding adhesive, honeycomb, adhesive bond between honeycomb and facesheets, and armor (shielding). In terms of a mathematical form, it can be written as

$$W_R = N(W_{HP}L_W + W_{HPADH} + W_{FSH} + W_{OSR} + W_{OSRADH} + W_{HC} + W_{HCADH} + W_{AR}) \quad (1)$$

Further, the radiator weight can be expressed as the product of the density and the thickness of each individual component. Equation (1) yields

$$W_R = L_W N\{W_{HP} + 4L_P(\rho t)_{HPADH} + 2\ell(\rho t)_{FSH} + \ell[(\rho t)_{OSR} + (\rho t)_{OSRADH} + (\rho t)_{AR}] + 2L_F[(\rho t)_{HC} + 2f(\rho t)_{HCADH}]\} \quad (2)$$

By performing a thermal energy balance on the system with the assumption of perfect view to space and constant fin root temperature, the actual radiator heat rejection can be expressed by[4]

$$q_R = 2L_W N(L_P + \eta L_F)\varepsilon\sigma T_R^4 \quad (3)$$

In addition, for radiator surfaces exposed to the sun, Earth, and other spacecraft appendages (antennas, solar array, etc.), an effective sink temperature T_s is defined such that

$$q_R = 2L_W N\left[L_P\varepsilon\sigma\left(T_R^4 - T_s^4\right) + \eta L_F\varepsilon\sigma T_R^4\right] \quad (4)$$

The ratio of the fourth power of effective sink temperature and heat pipe temperature are related to the dimensionless parameter θ by

$$\theta^4 = \frac{T_s^4}{T_R^4} = \left(\sum_i F_{R-i}\varepsilon_R\sigma T_i^4 + \alpha_s S\sin\theta_s + \alpha_s\rho_A S F_A + \varepsilon_R F_{IR}E_{IR}\right) \Big/ \sigma\varepsilon_R T_R^4 \quad (5)$$

The effectiveness η has been determined by solving the corresponding differential equation involving radiation and conduction terms.[5–7] Two different expressions for η have been correlated by various authors.[8,9] Chang[9] gives the following for a flat plate of constant cross section ($\delta = 1$):

$$\eta = (1 - 1.25\lambda + 1.6\lambda^2)(1 - \theta^4) \quad \text{for} \quad 0.01 \le \lambda \le 0.2 \quad (6a)$$

and

$$\eta = (0.5321 - 0.4049\log_{10}\lambda)(1 - \theta^4) \quad \text{for} \quad 0.2 \le \lambda \le 2.0 \quad (6b)$$

The parameters λ and θ are defined[5–7] as

$$\lambda = \frac{\varepsilon\sigma T_R^3 L_F^2}{k_F t_F} \quad (7)$$

and

$$\theta^4 = \frac{\alpha_s S\sin\theta_s}{\varepsilon\sigma T_R^4} \quad (8)$$

Equation (8) is a reduction of Eq. (5) to account for direct solar loads only; i.e., it is written for nonplanetary view satellite radiators without view of satellite appendages. In terms of these two parameters, Eq. (4) for the radiator heat rejection q_R can be rewritten as

$$q_R = 2L_W N\varepsilon\sigma T_R^4\left[L_P(1 - \theta^4) + \eta L_F\right] \quad (9)$$

By employing Eqs. (2) and (9) just derived, the equations governing the weight and the corresponding radiator area per unit heat rejection for various physical parameters can be stated as follows:

$$\frac{W_R}{q_R} = \frac{C_1 + \ell C_2 + L_F C_3}{2\varepsilon\sigma T_R^4\left[(1 - \theta^4)L_P + L_F\eta\right]} \quad (10)$$

$$\frac{A_R}{q_R} = \frac{L_P + L_F}{\varepsilon\sigma T_R^4\left[(1 - \theta^4)L_P + L_F\eta\right]} \quad (11)$$

It can also be shown from Eqs. (10) and (11) that

$$\frac{W_R}{A_R} = \frac{C_1 + L_F C_3}{\ell} + C_2 \quad (12)$$

Because the numerator of Eq. (10) increases with both ℓ and L_F while the denominator increases with L_F but decreases with η, there is some value of L_F that corresponds to a minimum value for W_R/q_R. Note that W_R is dependent on A_R and vice versa, as shown by Eq. (12). Because of this dependence, only one of the two quantities, W_R/q_R or A_R/q_R, may be minimized. In the present investigation, W_R/q_R is minimized.

To determine the optimum for the parameter L_F that produces the minimum value of weight per radiator heat rejection, Eq. (10) is minimized such that

$$\frac{\mathrm{d}}{\mathrm{d}L_F}\left(\frac{W_R}{q_R}\right) = 0 \quad (13)$$

$$\frac{\mathrm{d}^2}{\mathrm{d}L_F^2}\left(\frac{W_R}{q_R}\right) > 0 \quad (14)$$

Equations (13) and (14) are the necessary conditions for minimization. The result of this optimization is

$$(2C_2 + C_3)\left[L_P + L_F\eta/(1 - \theta^4)\right] - (C_1 + \ell C_2 + L_F C_3) \times (1 - 3.75\lambda + 8\lambda^2) = 0, \quad 0.01 \le \lambda \le 0.2 \quad (15)$$

$$(2C_2 + C_3)\left[L_P + L_F\eta/(1 - \theta^4)\right] - (C_1 + \ell C_2 + L_F C_3) \times (0.1804 - 0.4049\log_{10}\lambda) = 0, \quad 0.2 < \lambda \le 2.0 \quad (16)$$

The parameters L_F and λ are related by Eq. (7). The weight and the corresponding radiator area per unit heat rejection can be calculated from Eqs. (10) and (11) once the optimum fin length solution becomes available.

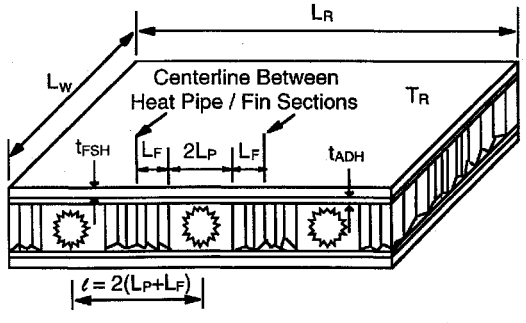

Fig. 1 Schematic diagram of a space radiator with embedded heat pipes.

Method of Solution

The resulting optimization equation, designated by either Eq. (15) or Eq. (16), is a fifth-degree equation in L_F that needs to be solved iteratively to find the real root that makes sense physically. In this study the nonlinear equations are solved by a Newton–Raphson numerical scheme.[10] Because the Newton–Raphson's global convergence properties are poor, a special fail–safe routine that utilizes a combination of bisection and Newton–Raphson is devised for this purpose. The hybrid algorithm takes a bisection step whenever Newton–Raphson would take the solution out of bounds, or whenever Newton–Raphson is not reducing the size of the brackets rapidly enough. Once the smallest root L_F is available from the solution, which is obtained from iterating within a prescribed error band, the minimum weight and the corresponding radiator area can be determined on a per unit heat rejection basis with Eqs. (9) and (10) from various physical parameters.

The computer program is written in Fortran 77 on the Sun SPARCstation 10 that rapidly solves the equations. The accuracy of the algorithm was verified by comparing results[9] for some selected cases. The close agreement confirms that the proposed model is effective for weight optimization for honeycomb radiators with embedded heat pipes.

Results

The results are presented as a function of radiator weight to heat rejection for a corresponding radiator area per heat rejection. This allows an optimal weight trade to be made as a function of permissible parameter variations. The results presented here are limited to direct solar heating, but several such parameters including the environment effect of reflective solar heating, planetary emission and albedo, and infrared heating from spacecraft appendages can be quantified. Additionally, changes in sun angle and planetary view factors because of spacecraft attitude can be assessed.

The constant material properties and dimensions used for the analysis of a space radiator panel with embedded heat pipe are as follows:

f	= 1.0
k	= 0.176 kW/m-K (102 Btu/h-ft-°F) for Al-6061
k	= 0.154 kW/m-K (89 Btu/h-ft-°F) for P120
k	= 0.917 kW/m-K (530 Btu/h-ft-°F) for K1100
L_P	= 7.94E-3 m (0.3125 in.)
S	= 1.419 kW/m^2 (450 Btu/h-ft^2)
t_{ADH}	= 1.02E-4 m (0.004 in.)
t_{AR}	= 0 m (0.0 in.)
t_F	= 5.08E-4 m (0.020 in.)
t_{HC}	= 1.59E-2 m (0.625 in.)
t_{OSR}	= 2.03E-4 m (0.008 in.)
W_P	= 0.373 kg/m (0.251 lb/ft)
ε	= 0.79
ρ_{ADH}	= 1.20E3 kg/m^3 (75 lb/ft^3)
ρ_{AR}	= 0 kg/m^3 (0 lb/ft^3)
$\rho_{Al\text{-}6061}$	= 2.71E3 kg/m^3 (169 lb/ft^3)
ρ_{HC}	= 3.69E1 kg/m^3 (2.3 lb/ft^3)
ρ_{K1100}	= 1.82E3 kg/m^3 (113.7 lb/ft^3)
ρ_{OSR}	= 2.21E3 kg/m^3 (137.5 lb/ft^3)
ρ_{P120}	= 1.67E3 kg/m^3 (104.2 lb/ft^3)

Figure 2 illustrates the improvement potential of the use of P120 and K1100 materials vs a commonly used aluminum 6061 facesheet material. However, this is based on in-plane thermal conductivity of the composite. The thermal conductivity normal to the in-plane fiber direction in these composite materials is, in the case of the K1100, approximately one-fourth that of aluminum. This effect on the panel efficiency or out-of-plane temperature gradient is not accounted for in this paper. Structurally, development is required to qualify these and similar composite materials as in equipment-mounted radiator panels to take advantage of the relatively high specific thermal conductivity, k/ρ. If this can be accomplished then significant weight savings might be realized.

Figures 3a, 3b, 4a, and 4b for the baseline aluminum system compare the weight and area effects of solar incidence angle θ_s at 10 and 23.5 deg vs solar absorptance for the range of typical radiator temperatures. It can be readily seen that there is significant weight and area impact between typical beginning-of-life (BOL) α_s values of 0.10 compared to values of 0.2–0.4 for end-of-life (EOL) radiators. This is most pronounced at $\theta_s = 23.5$ deg and low radiator

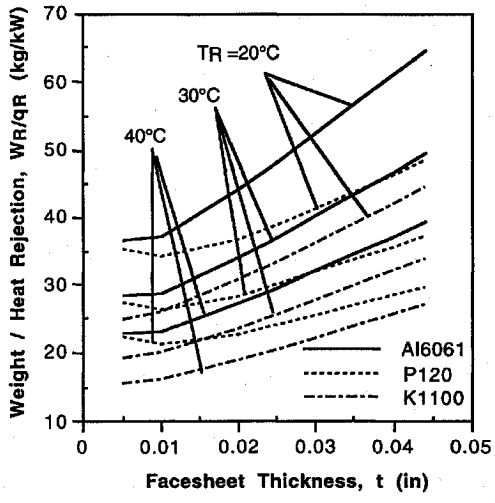

Fig. 2 Weight optimization for selected facesheet materials with θ_s = 23.5 deg and α_s = 0.32 at various heat rejection temperatures.

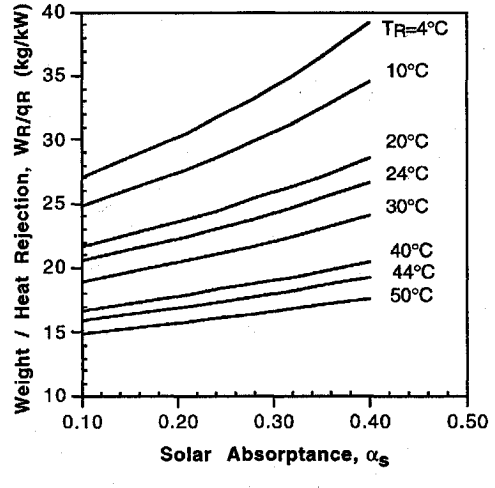

Fig. 3a Weight optimization for Al-6061 facesheet and θ_s = 10 deg at various heat rejection temperatures.

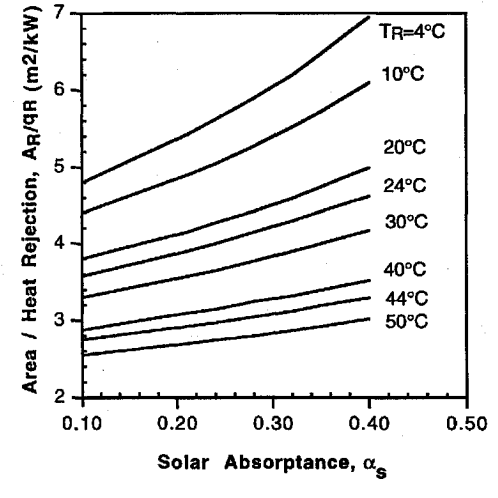

Fig. 3b Area corresponds to optimized weight for Al-6061 facesheet and θ_s = 10 deg at various heat rejection temperatures.

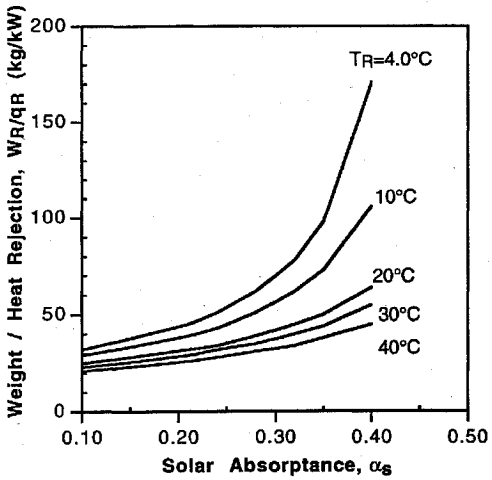

Fig. 4a Weight optimization for Al-6061 facesheet and θ_s = 23.5 deg at various heat rejection temperatures.

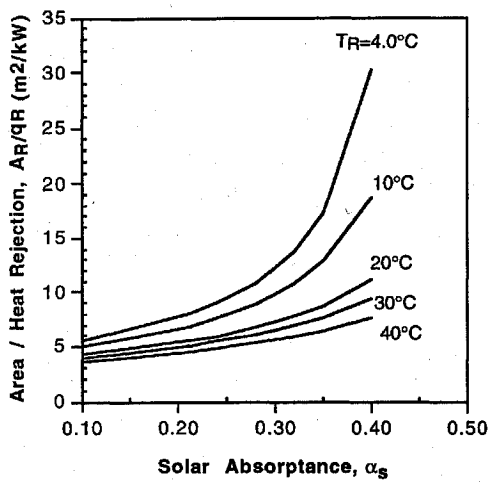

Fig. 4b Area corresponds to optimized weight for Al-6061 facesheet and θ_s = 23.5 deg at various heat rejection temperatures.

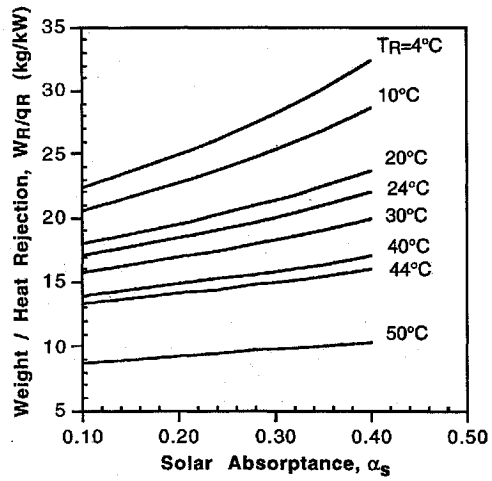

Fig. 5a Weight optimization for P120 facesheet and θ_s = 10 deg at various heat rejection temperatures.

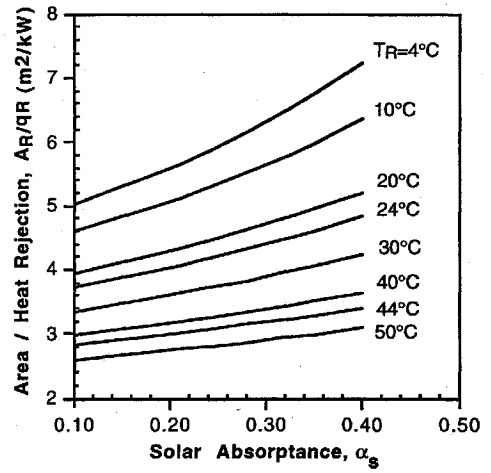

Fig. 5b Area corresponds to optimized weight for P120 facesheet and θ_s = 10 deg at various heat rejection temperatures.

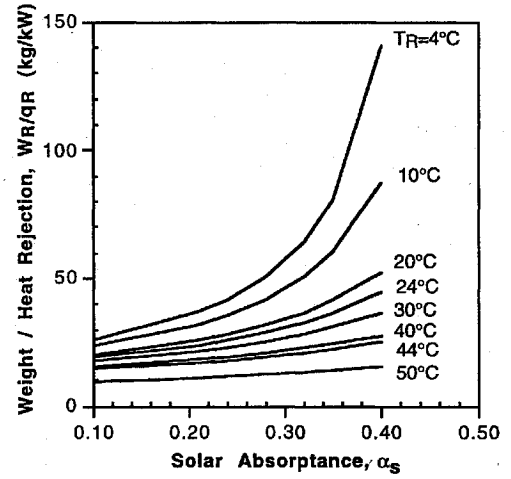

Fig. 6a Weight optimization for P120 facesheet and θ_s = 23.5 deg at various heat rejection temperatures.

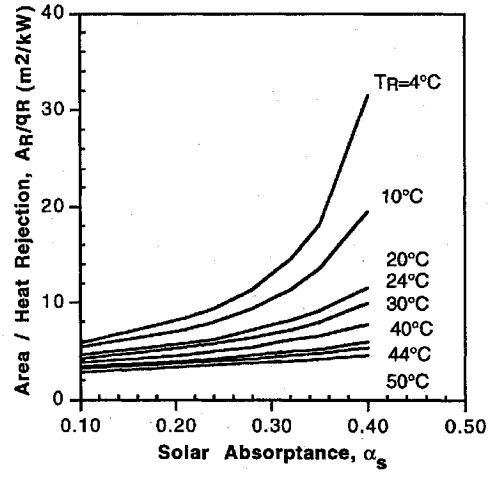

Fig. 6b Area corresponds to optimized weight for P120 facesheet and θ_s = 23.5 deg at various heat rejection temperatures.

temperature requirements. The influence of contamination levels and uncertainty margin requirements as well as temperature level requirements is also evident. Figures 5a, 5b, 6a, and 6b compare the same effects as Figs. 3a, 3b, 4a, and 4b except the aluminum facesheets have been replaced with P120 composite of the same thickness (0.020 in.).

Figures 7 and 8 compare the weight savings as a function of facesheet root temperature and solar incidence angle with the latter showing the influence of radiator temperature requirements that are dependent on equipment temperature level requirements and design uncertainty requirements.

Figure 9 illustrates the impact of facesheet surface emittance between typical OSR values of 0.75–0.8 and emittance enhancements through surface coatings in the range of 0.8–0.85. Higher values are possible for white paints in the range of 0.9–0.93 but are not effective unless the solar incidence angle can be significantly reduced to lower the influence of higher solar absorptance. White paint

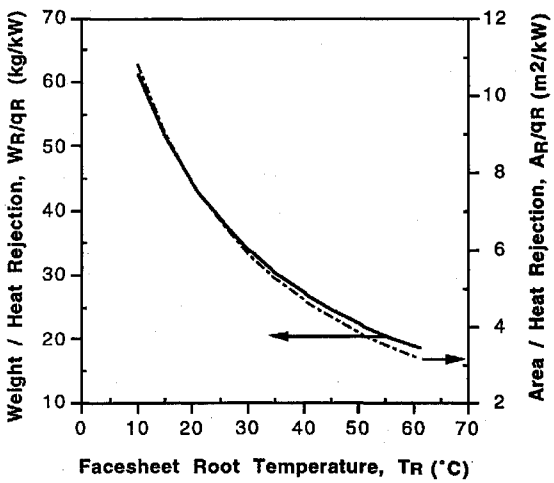

Fig. 7 Weight optimization and corresponding area for Al-6061 facesheet, $\theta_s = 23.5$ deg and $\alpha_s = 0.32$ as a function of facesheet root temperature.

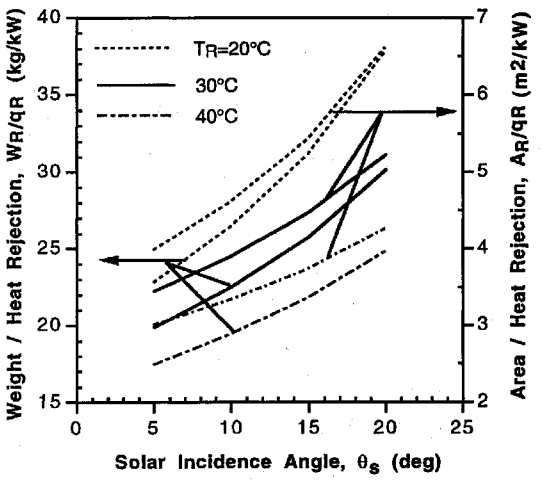

Fig. 8 Weight optimization and corresponding area for Al-6061 facesheet and $\alpha_s = 0.32$ at various facesheet root temperatures as a function of solar incidence angle.

absorptances for BOL conditions have been reported in the 0.12–0.15 range as compared with 0.06–0.1 for OSRs, but the EOL values for both materials are functions of material stability and overall contamination levels that also are influenced by orbit altitude/space environment.

The effects of worst-case solar absorptance and sun angle are presented in numerical form for comparison. To illustrate some of these effects on weight optimization, case runs were made varying the thermal control coating radiative property (α/ε) that are independent characteristics of materials and/or contamination levels. Hence, the radiative effects of material surface property changes and reduction of contamination levels can be quantified. Table 1 presents the weight and area impact for several radiator configurations as functions of the sun angle and solar absorptance. The baseline configuration with Al-6061 facesheet is documented as cases 1 and 2 for 8- and 4-mil OSR, respectively. Also shown are the changes in radiator fin effectiveness through the use of lightweight facesheet materials such as composites (cases 3 and 4). Besides these effects, the parasitic heat load of the radiator resulting from direct solar exposure is shown as a function of sun angle and solar absorptance. The results shown in Table 1 can be compared to demonstrate these alternate effects on required weight and area per kilowatt of heat rejection. Tradeoffs can therefore be made, for example, based on propulsion usage for attitude control or switching between sunlit and nonsunlit radiators vs improved heat rejection capability. It should be noted that the area differences in cases 1 and 2 are probably because of solution round-off error as the coating thickness does not affect the required area as the emittance is

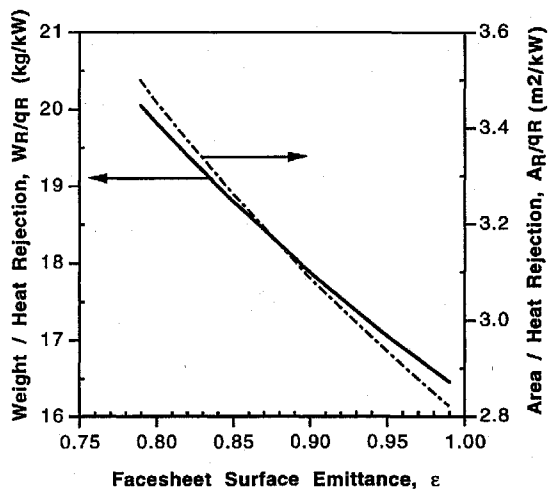

Fig. 9 Weight optimization and corresponding area for Al-6061 facesheet, $T_R = 20°C$, $\theta_s = 23.5$ deg, and $\alpha_s = 0.32$ as a function of facesheet surface emittance.

assumed constant. However, in cases 3 and 4 both the facesheet thermal conductivity and the density are different so that the area differences are real.

Another effect that can be assessed is the weight penalty associated with a temperature margin requirement. Traditionally government programs have required the use of 11°C uncertainty margin whereas commercial programs have used 5–7°C that translates directly to acceptable radiator temperature level requirements. Hence, several temperature levels are included in Table 1 (including those differing by 6°C) to show this weight penalty. The results are shown in cases 5–8. The weight clearly demonstrates that the thermal margin is a significant factor in spacecraft thermal control design.

To more clearly illustrate the information presented in Table 1, weight and area differences (penalties) were determined for three environmental conditions (A, B, and C) of sun angle and EOL solar absorptance. These penalties are listed in Table 2 for each of the eight design cases. Condition A assumes that the incident sun angle can be maintained at 10 deg by suitable satellite maneuvering and the effect of changing from an EOL solar absorptance of the radiator of 0.2–0.3 is desired. The EOL value of 0.3 is based on OSR data typical for a geosynchronous orbit.[11,12] However, if the self-contamination of satellites can be reduced, then EOL values of 0.2 or lower can be realized. The weight and area penalties range from −0.93 to −3.15 kg/kW and from −0.16 to −0.55 m^2/kW, respectively. The weight and area effects are most pronounced as the radiator temperature requirement is lowered to accommodate temperature-sensitive equipment and thermal uncertainty margin.

Condition B results show the increased effects of incident sun angle of 23.5 deg for the summer or winter solstice on a corresponding north or south facing radiator of a typical 3-axis inertially stabilized satellite. The weight/area penalties are much more significant because the incident solar load increases by 2.3 (θ_s changes from 10 to 23.5 deg). The weight penalties vary from −3.25 to −17.88 kg/kW and the corresponding area penalties range from −0.56 to −3.15 m^2/kW.

The condition C results present the combined effects of both the sun angle and the EOL contamination level. The results show the substantial impact if both sun angle and contamination levels can be reduced through maneuvering and design changes such as vent path control, use of low volatile condensible materials and on-orbit cleaning operations. The weight and area penalties range from −5.91 to −27.89 kg/kW and from −1.01 to −4.91 m^2/kW, respectively. Although the greatest impact is for low-temperature radiator panels at 10°C, it is seen that even for panels typically operating at 30°C, the weight and area penalty is −11.76 and −2.04 m^2/kW, respectively.

To evaluate the feasibility of any of these potential satellite thermal design modifications, it will be necessary to perform a cost-benefit analysis. However, a rough order-of-magnitude saving can be readily obtained using the weight savings for those payloads

Table 1 Weight and area impact for several radiator configurations[a]

Design case	Sun angle, θ_s: 10 deg W_R/q_R, kg/kW	10 deg A_R/q_R, m²/kW	23.5 deg W_R/q_R, kg/kW	23.5 deg A_R/q_R, m²/kW	10 deg W_R/q_R, kg/kW	10 deg A_R/q_R, m²/kW	23.5 deg W_R/q_R, kg/kW	23.5 deg A_R/q_R, m²/kW
1. Baseline configuration Al-6061 facesheet synchronous orbit 100% view to space $T_R = 30°C$	20.39	3.53	25.30	4.38	22.04	3.82	32.15	5.57
2. Al-6061 microsheet 4 mil OSR, $T_R = 30°C$	19.10	3.55	24.31	4.41	21.18	3.84	30.90	5.60
3. P120 facesheet $T_R = 30°C$	16.90	3.60	20.97	4.47	18.27	3.89	26.65	5.68
4. K1100 facesheet $T_R = 30°C$	14.07	3.40	17.46	4.21	15.21	3.67	22.19	5.36
5. Al-6061 facesheet $T_R = 10°C$	27.41	4.83	37.42	6.59	30.56	5.38	55.30	9.74
6. Al-6061 facesheet $T_R = 19°C$	23.88	4.17	31.03	5.42	26.21	4.58	42.23	7.38
7. Al-6061 facesheet $T_R = 25°C$	21.88	3.81	27.68	4.81	23.81	4.14	36.17	6.29
8. Al-6061 facesheet $T_R = 50°C$	15.65	2.67	18.31	3.12	16.58	2.83	21.56	3.68
Absorptance, α_s	0.2				0.3			

[a]Where $t_{OSR} = 8$ mil except noted otherwise.

Table 2 Weight and area penalties from Table 1 design cases for several environmental conditions

Design case	Environmental conditions: Condition A ($\theta_s = 10$ deg, α_s increases from 0.2 to 0.3) $\Delta(W_R/q_R)$, kg/kW	Condition A $\Delta(A_R/q_R)$, m²/kW	Condition B ($\theta_s = 23.5$ deg, α_s increases from 0.2 to 0.3) $\Delta(W_R/q_R)$, kg/kW	Condition B $\Delta(A_R/q_R)$, m²/kW	Condition C (θ_s increases from 10 to 23.5 deg, α_s increases from 0.2 to 0.3) $\Delta(W_R/q_R)$, kg/kW	Condition C $\Delta(A_R/q_R)$, m²/kW
1	−1.65	−0.29	−6.85	−1.19	−11.76	−2.04
2	−2.08	−0.29	−6.59	−1.19	−11.80	−2.05
3	−1.37	−0.29	−5.68	−1.21	−9.75	−2.08
4	−1.14	−0.27	−3.39	−1.15	−8.12	−1.96
5	−3.15	−0.55	−17.88	−3.15	−27.89	−4.91
6	−2.33	−0.41	−11.20	−1.96	−18.35	−3.21
7	−1.93	−0.33	−8.49	−1.48	−14.29	−2.48
8	−0.93	−0.16	−3.25	−0.56	−5.91	−1.01

launched on the Ariane where the cost per kilogram of payload is a linearly increasing function. However, for other launch vehicles, payload weight savings might enable the spacecraft designer to choose a smaller launch vehicle (or smaller boost configuration) with consequent savings. Of course, these cost savings will be offset by the cost of design modification and potentially increased on-board fuel for maneuvering, and so a tradeoff will be required for any proposed plan.

Conclusions

A space radiator optimization program has been developed for a thermal technology tradeoff study. The mathematical model is based on a steady-state analytical relationship expressing minimum radiator weight per unit heat rejection with corresponding radiator area per unit heat rejection to allow optimal weight trade as a function of parameter variations. The program developed in this study can be used as a tool to analyze the thermal performance of embedded heat pipe spacecraft radiator panels. It allows logical study of the effects of environmental parameters such as direct and reflective solar heating, Earth emission and albedo, and infrared heating from spacecraft appendages. Changes in sun angle and planetary view factors because of spacecraft attitude including changes in thermal control coating solar absorptance and infrared emittance because of material differences or contamination effects are easily accommodated. The radiator fin effects of material changes in facesheets such as the use of new composite materials are included as well as weight effects of thermal control coatings, armor (shielding), adhesive layers, honeycomb materials, and heat pipes. Optimal heat pipe spacing is calculated for the optimal weight solution together with the corresponding area per unit heat dissipation or payload heat rejection capability.

The radiator weight optimization program provides an efficient tool for thermal technology tradeoff studies to determine the effects of various potential radiator improvements. The graphical data presented in this study are applicable to practical engineering design application.

References

[1]Mertesdorf, S. J., "Development of a Generalized Radiator Weight Optimization Design Code for High Power Spacecraft Applications," AIAA Paper 86-1268, June 1986.

[2]Muller, R., Rieck, U., Koppl, A., and Stramaccioni, D., "Design and Test of a Honeycomb Radiator Panel with Carbon Fiber Reinforced Plastic Facesheets and Aluminum Heat Pipes," Society of Automotive Engineers, SAE TP Series 932302, Warrendale, PA, July 1993.

[3]Kelly, W. H., and Reisenweber, J. H., "Thermal Performance of Embedded Heat Pipe Spacecraft Radiator Panels," Society of Automotive Engineers, SAE TP Series 932158, Warrendale, PA, July 1993.

[4]Anon., "Radiator Design for Space Vehicles," AiResearch Manufacturing Co., Pub. MS-AP 0069, Los Angeles, CA, June 1963.

[5]Lieblein, S., "Analysis of Temperature Distribution and Radiant Heat Transfer Along a Rectangular Fin of Constant Thickness," NASA TN D-196, Nov. 1959.

[6]Bartas, J. G., and Sellers, W. H., "Radiation Fin Effectiveness," *Journal of Heat Transfer*, Vol. 82, Feb. 1960, pp. 73–75.
[7]Mackay, D. B., "Space Radiator Analysis and Design," Space and Information Systems Div., North American Aviation, ASD TR 61-30, Downey, CA, Dec. 1961.
[8]Truong, H. V., and Mancuso, R. J., "Performance Predictions of Radiating Annular Fins of Various Profile Shapes," American Society of Mechanical Engineers, ASME Paper 80-HT-31, New York, July 1980.
[9]Chang, H. V., "Optimization of a Heat Pipe Radiator Design," AIAA Paper 84-1718, June 1984.
[10]Acton, F. S., *Numerical Methods That Work*, Mathematical Association of America, corrected ed., Washington, DC, 1990, Chap. 2.
[11]Curran, D. G. T., and Millard, J. M., "Results of Contamination /Degradation Measurements on Thermal Control Surfaces of an Operational Satellite," AIAA Paper 74-740, June 1977.
[12]Stewart, T. B., Arnold, G. S., Hall, D. F., Marvin, D. C., Hwang, W. C., Young Owl, R. C., and Marten, H. D., "Photochemical Spacecraft Self-Contamination: Laboratory Results and System Impacts," *Journal of Spacecraft and Rockets*, Vol. 26, No. 5, 1989, pp. 358–367.

I. E. Vas
Associate Editor